CARBON 48 (2010) 4351–4361

available at www.sciencedirect.com

ScienceDirect

journal homepage: www.elsevier.com/locate/carbon

High voltage supercapacitor built with seaweed carbons in neutral aqueous electrolyte

M.P. Bichat, E. Raymundo-Piñero, F. Béguin *

Centre de Recherche sur la Matière Divisée, CNRS/University, 1B Rue de la Férollerie, 45071 Orléans, France

ARTICLE INFO

Article history:
Received 13 March 2010
Accepted 28 July 2010
Available online 3 August 2010

ABSTRACT

High oxygen content (10–15 at.%) nanotextured carbons were obtained by pyrolysis of seaweeds at 600–750 °C and applied as electrodes for supercapacitors in H_2SO_4, KOH and Na_2SO_4 aqueous media. Interestingly, the potential stability window measured in a three-electrode cell configuration depends both on the nature of the oxygenated surface functionality and on the electrolyte pH. A high value of 2.4 V was observed in Na_2SO_4 for the seaweeds pyrolysed at 600 °C, showing that the surface functionality strongly influences the over-potentials of di-hydrogen evolution and carbon oxidation. Symmetric capacitors built from the seaweed carbons exhibited an excellent cycle life for voltage values up to 1.6 V, showing the promise of Na_2SO_4 for developing high energy density and environment friendly systems.

1. Introduction

In the last decade, carbon materials, owing to their low cost, good electrical conductivity, developed porosity and possibility of tailoring the nanotexture and chemical composition, gained an interest in supercapacitor applications [1,2]. Carbon/carbon supercapacitors present higher power density and longer cycle life [3,4] than accumulators.

For a supercapacitor, the amount of energy (E) stored is related to the capacitance (C) and voltage (U) according to the relation: $E = 1/2CU^2$. In industry, the organic electrolyte is preferred because the voltage applied between the electrodes is higher (~2.7 V) than with aqueous electrolyte (~1 V) [5]. In aqueous electrolyte, however, the amount of energy stored can be enhanced either by applying materials developing higher capacitance or by increasing the operating voltage. In the particular case of capacitance, it can be significantly improved through pseudo-faradic reactions between the aqueous electrolyte and active groups present on the carbon surface [3,6,7].

Several routes are already mentioned in the literature to obtain heteroatom-rich nanoporous carbons. Foreign atoms such as oxygen can be introduced on the carbon surface by different oxidation procedures using an oxygen atmosphere [7], a plasma treatment [8] or chemical oxidation by HNO_3 [9]. Nitrogen enrichment can be performed by ammoxidation or by reaction with urea [10]. Heteroatom rich carbons can also be obtained by the pyrolysis of a suitable oxygen or nitrogen containing precursor, with or without a template [11–15]. For example, we have previously shown that one-step carbonization of biopolymers extracted from seaweeds or seaweeds themselves results in high oxygen content nanotextured carbons [13,16]. Such carbons, owing to their high amount of oxygenated surface functionalities (10–15 at.% oxygen), present high capacitance values (250 F g^{-1}) in spite of their low specific surface area (400–700 m^2 g^{-1}), and a broad stability potential window in 1 mol L^{-1} H_2SO_4. Symmetric capacitors built with the seaweed based nanoporous carbons are able to be reversibly charged/discharged more than 10,000 times in a voltage window of 1.2 V. They outperform the activated

* *Corresponding author:*
E-mail address: beguin@cnrs-orleans.fr (F. Béguin).
0008-6223/$ - see front matter © 2010 Elsevier Ltd. All rights reserved.
doi:10.1016/j.carbon.2010.07.049

carbon based ones which can be polarized only up to 0.8–1.0 V [5] in this medium.

Unfortunately, the use of H_2SO_4 as electrolyte presents many technical drawbacks precluding its industrial application, mainly due to its corrosive character towards the different metallic components of a supercapacitor, e.g., current collectors, connexions, can, etc. Other electrolytes as KOH or Na_2SO_4 could be in turn more compatible for the supercapacitor industry. Actually, KOH is implemented as electrolyte in alkaline batteries (Ni–MH) where nickel and copper current collectors are used for positive and negative electrodes, respectively [17]. The possibility of enhancing the capacitance of carbon materials through fast redox reactions involving N and O surface functionalities has been already proved in this medium [7,10,12]. Neutral electrolytes have been used for asymmetric systems based on metallic oxide and activated carbon for positive and negative electrode, respectively [18,19]. Few studies on three-electrode cell performance of activated carbons in Na_2SO_4 show that the pseudo-faradic redox transitions of O and N-containing electroactive surface groups are depressed in comparison with H_2SO_4 [20–24].

In this report, we present the electrochemical performance of symmetric capacitors with seaweed carbon electrodes in KOH and Na_2SO_4 electrolytes. A detailed study in three- and two-electrode cells, varying the porous texture and surface functionality, shows that Na_2SO_4 performs particularly well. In this medium, the stability potential window of seaweed based carbons is wider than in KOH or even H_2SO_4. As a consequence, symmetric capacitors are able to operate reversibly up to 1.6 V in this environment friendly and less corrosive medium.

2. Experimental

2.1. Samples preparation

The brown seaweed *Lessonia nigrescens* (LN) has been used as carbon precursor. In order to get the carbon materials, the dried seaweed was pyrolyzed in a tubular furnace under nitrogen flow (100 mL min^{-1}) up to 600 or 750 °C. The heating rate was 10 °C min^{-1} and the maximum temperature was hold for 3 h. The resulting black solid was then thoroughly washed 5 times with 5 mol L^{-1} HCl for 24 h at 80 °C and 5 times in distilled water, in order to make sure that a neutral pH is reached. Afterwards, the material was dried at 120 °C overnight in an oven. The carbons obtained at 600 and 750 °C are named LN600 and LN750, respectively.

2.2. Physico-chemical characterization of the carbon samples

The porous texture of the various carbons has been analyzed by N_2 and CO_2 adsorption at 77 and 273 K, respectively (Autosorb-1, Quantachrome). Before the measurements, the samples were outgassed at 200 °C overnight under vacuum. The specific surface area was calculated from the nitrogen adsorption isotherms by applying the BET and Dubinin–Radushkevich equations. The non-linear density functional theory (NLDFT) method was applied to the N_2 adsorption isotherms to determine the pore size distribution. The micro and mesopore volumes were determined from the N_2 adsorption isotherms by applying the NLDFT equation. The ultramicropore volume and surface area were obtained by applying the Dubinin–Radushkevich equation to the CO_2 adsorption data. The surface functionality of the carbon materials was analyzed by X-ray photoelectron spectroscopy (XPS) using a VG ESCALAB 250 spectrometer with an AlKα monochromatic source (15 kV, 15 mA) and a multidetection analyzer under a residual pressure of 10^{-8} Pa. The analyses have been performed either on the as-received carbon powders or after wetting the carbon materials with the electrolytic solution (6 mol L^{-1} KOH or 0.5 mol L^{-1} Na_2SO_4) during 24 h under stirring followed by a thorough washing in distilled water and drying.

2.3. Electrochemical measurements

Composite electrodes (10–12 mg) in the form of 1 cm^2 pellets were pressed from a mixture of seaweed based carbon (90 wt.%) and a binder (polyvinylidene fluoride PVDF: 10 wt.%). The experiments were performed in two- or three-electrode Teflon Swagelok® systems using a glassy fibrous separator and gold current collectors. For the three-electrode cells, the counter electrode was a graphite rod and the reference electrode was Hg/Hg_2SO_4 (0.62 V/NHE) or Hg/HgO (0.098 V/NHE) in 0.5 mol L^{-1} Na_2SO_4 and 6 mol L^{-1} KOH, respectively. All the potential values of the study are reported *vs* the normal hydrogen electrode (NHE). Electrochemical measurements were performed using a VMP multichannel potentiostat/galvanostat (Biologic, France). The electrochemical performance of the two materials was evaluated by cyclic voltammetry (CV) at 2 mV s^{-1} and galvanostatic charge/discharge at 200 mA g^{-1}.

3. Results and discussion

3.1. Physico-chemical characterization of the carbon samples

The nitrogen adsorption isotherms and the pore size distribution (PSD) for LN600 and LN750 are plotted in Fig. 1. The type IV isotherms with an hysteresis loop at $P/P_0 > 0.4$ are characteristic of samples with micropores and mesopores. The specific surface area and pore volumes obtained from the adsorption measurements are listed in Table 1. The samples exhibit moderate values of BET specific surface area (750–1080 m^2 g^{-1}). The DR specific surface areas estimated from the CO_2 and N_2 isotherms are comparable, indicating that the micropores are mostly in the range 0.7–0.8 nm [25]. The contribution of mesopores is rather significant (Table 1 and Fig. 1) with pores in the range 2–4 nm.

The increase of the pyrolysis temperature from 600 to 750 °C does not only result in a somewhat more developed porosity but it also affects significantly the surface functionality. The XPS data (Table 2) reveal that both nitrogen and oxygen contents are reduced when the pyrolysis temperature is increased. The chemical nature of the oxygenated functional groups was determined by deconvolution of the C1s peak

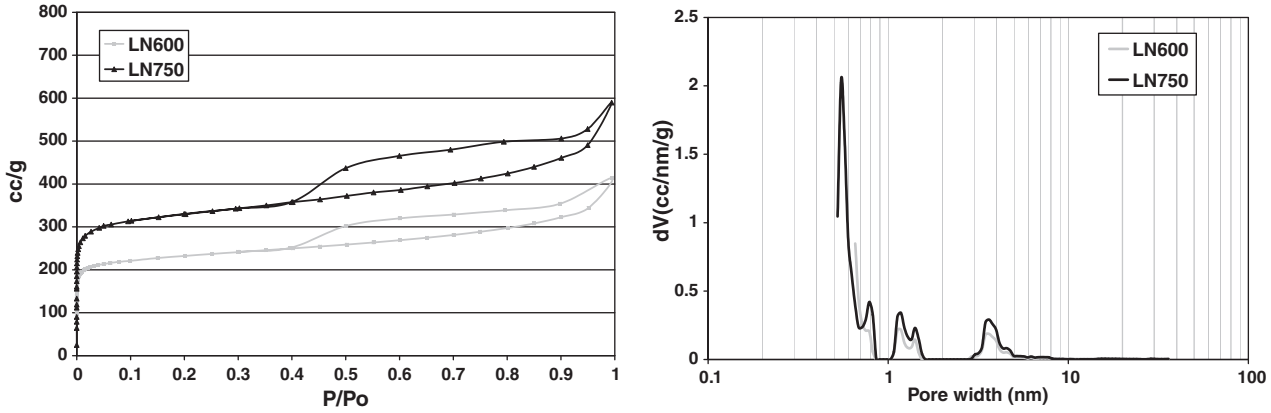

Fig. 1 – N_2 adsorption isotherms (left) and NLDFT pore size distribution (right) for LN600 and LN750.

Table 1 – Specific surface area and pore volume of the seaweed based carbons.

Sample	S_{BET} (N_2) ($m^2\ g^{-1}$)	S_{DR} (N_2) ($m^2\ g^{-1}$)	S_{DR} (CO_2) ($m^2\ g^{-1}$)	$V_{ultramicro}$ [a] ($d < 0.7$ nm) ($cm^3\ g^{-1}$)	V_{micro} [b] ($d < 2$ nm) ($cm^3\ g^{-1}$)	V_{meso} [b] ($2 < d < 50$ nm) ($cm^3\ g^{-1}$)
LN600	746	1061	1001	0.38	0.29	0.30
LN750	1082	1351	1480	0.57	0.40	0.40

a obtained after applying the Dubinin–Radushkevich equation to the CO_2 adsorption data,
b obtained after applying the DFT method to the N_2 adsorption data.

Table 2 – XPS surface characterization of the as-received LN carbons.

Sample	O at.%	N at.%	C–OR (286.3 ± 0.2 eV) at.%	C=O (287.5 ± 0.2 eV) at.%	–O–C=O (289.0 ± 0.2 eV) at.%
LN600	11.5	2.6	4.2	2.0	2.5
LN750	7.3	1.4	3.1	1.2	1.5

(Table 2). The groups detected on the surface of the LN samples are, from the most to the least represented, ether and phenol (C–OR), carboxylic groups (–O–C=O), quinone and ketone (C=O).

Taking into account earlier studies by Boehm and Voll [26], where oxygen chemisorption is described when a carbon material is immersed into an aqueous solution containing di-oxygen, the surface functionality of the LN-based carbons was analyzed by XPS after 24 h immersion in the electrolytes (6 mol L^{-1} KOH and 0.5 mol L^{-1} Na_2SO_4). By such analysis, one has a direct access to the nature of the surface functionality in the experimental conditions of the electrochemical tests. After contact with both electrolytes, the amount of surface oxygen is dramatically increased whereas the nitrogen content remains unchanged (Table 3). Comparing the results obtained for LN600 and LN750 before (Table 2) and after (Table 3) immersion in the electrolyte, it appears clearly that new oxygenated functionalities are created on the carbon surface by contact with the electrolyte. In particular, the amount of C–OR type functionalities, probably phenol groups, is considerably enhanced whatever the electrolyte.

By contrast, if the carbon powders are wetted in the same conditions using a degassed (O_2-free) Na_2SO_4 solution, the oxygen content measured by XPS is 11.0 and 9.8 at.% for LN600 and LN750, respectively, i.e. comparable with the values for the as-received powders (Table 2). These results confirm the role of dissolved di-oxygen on carbon surface oxidation when the solutions are not degassed. Such effect does not occur when the samples are exposed to di-oxygen from the atmosphere because these redox reactions require

Table 3 – XPS analysis of LN carbons after immersion in an electrolyte.

Sample	Electrolyte	O at.%	N at.%	C–OR (286.3 ± 0.2 eV) at.%	C=O (287.5 ± 0.2 eV) at.%	–O–C=O (289.0 ± 0.2 eV) at.%
LN600	KOH	15.0	3.2	6.3	2.5	3.1
LN750	KOH	11.8	1.3	5.5	1.5	2.2
LN600	Na_2SO_4	15.8	2.4	6.9	2.2	3.5
LN750	Na_2SO_4	12.8	1.9	6.1	1.2	2.8

a simultaneous exchange of electrons and protons. The interaction mechanism between an active carbon surface and electrolyte solutions has been studied in the past (see reviewed literature in [27]) but it was not unequivocally explained.

From the foregoing, in order to interpret electrochemical results obtained in aqueous electrolytes, it is very important to know how the cells are prepared. For all the experiments presented in this work, the electrolyte solutions were not outgassed before the electrochemical measurements. Therefore, the surface functionality presented in Table 3 should be considered for further correlations to the electrochemical behaviour of each material.

3.2. Electrochemical characterization of the carbon samples

3.2.1. Three-electrode cell characterization using different aqueous electrolytes

Fig. 2 shows the cyclic voltammogramms (CV) of LN600 and LN750 in three-electrode cells with 1 mol L^{-1} H_2SO_4 (Fig. 2a), 6 mol L^{-1} KOH (Fig. 2b) and 0.5 mol L^{-1} Na_2SO_4 (Fig. 2c). On the left side, the CVs are comprised totally (Fig. 2a, left) or almost totally (Fig. 2b and c, left) within the thermodynamic stability window of water. The latter is represented in all figures by two vertical lines corresponding to the potentials of water reduction and oxidation, respectively. On the right side of Fig. 2, the CVs have been recorded in the total stability window of the system.

In all electrolytes, LN750 displays more rectangular voltammograms than LN600, confirming a higher electrical conductivity for LN750 as a consequence of the higher pyrolysis temperature.

Within the stability window of water (Fig. 2, left), the capacitive response includes charging of the electrical double-layer (EDL) and the pseudo-faradic contribution of the surface functionality. Due to the richer surface functionality of LN600 compared to LN750 (Table 3), reversible redox humps are observed for LN600, independently of the electrolyte used, while such humps are almost undetectable in the case of LN750.

In H_2SO_4, the cathodic and anodic peaks are placed at around 0.3 and 0.6 V *vs* NHE, respectively (Fig. 2a, left). These peaks, generally attributed to the reversible quinone/hydroquinone transformation [16,28], are the most pronounced for LN600 with the highest amount of quinone-like functionalities (C=O in Table 3). Due to these pseudo-faradic reactions, the capacitance is more important for LN600 (244 F g^{-1}) than for LN750 (209 F g^{-1}), even if the specific surface area of LN600 is lower than for LN750 (see Table 1).

In KOH (Fig. 2b, left) the cathodic/anodic peaks related to the reduction/oxidation of oxygenated functionalities are placed at −0.5 and −0.3 V *vs* NHE, respectively. When the pH of the electrolytic solution is increased, the redox reactions involving surface quinone groups are less important, but some other surface functionalities as pyrone-like ones can be active [27]. Since LN600 posses more pyrone like functionalities than LN750 (see the higher amount of C–O and C=O-like groups in Table 3), it can deliver a higher capacitance (206 F g^{-1}) than LN750 (186 F g^{-1}).

Finally, for LN600 in Na_2SO_4 (Fig. 2c, left), the cathodic/anodic redox humps appear at −0.1 and 0.1 V *vs* NHE, respectively. As a consequence, LN600 presents a slightly higher capacitance (121 F g^{-1}) than LN750 (115 F g^{-1}). Taking into account the lower specific surface area of LN600, it confirms that pseudo-faradic reactions contribute to the capacitance of this material in Na_2SO_4. Although Andreas and Conway [28] stated that the pseudo-capacitive contribution of surface oxygenated groups is negligible at neutral pH, from these data on the two materials prepared from the same precursor, we can affirm that pseudo-faradic reactions are possible in Na_2SO_4 with an adequate surface functionality. In this sense, LN600 contains a higher amount of all kinds of functionalities (Table 3) than LN750, particularly the quinone-like groups (C=O) which are twice more present than in LN750.

When comparing the results in the three electrolytes, it can be also pointed out that LN600 and LN750 exhibit smaller capacitance values in Na_2SO_4 than in H_2SO_4 and KOH. Such results are in agreement with the literature data stating that the EDL capacitance values are higher in H_2SO_4 than in Na_2SO_4 because of the presence of protons as mobile species with better ionic diffusion inside the pores than other ions [21,22]. A similar interpretation can be given for understanding the capacitance differences obtained in KOH and Na_2SO_4, the hydroxyl ions being the mobile species in this case. Actually, the conductivity of the 0.5 mol L^{-1} Na_2SO_4 solution has been found to be 60 mS cm^{-1}, which is approximately one order of magnitude less than in the H_2SO_4 and KOH solutions considered in this study. Nevertheless, the influence of pH and/or electrolyte ions on the EDL capacitance is not an easy issue and some work is still necessary in this direction.

In aqueous electrolyte, when the potential range is extended to more negative values, a second redox contribution due to hydrogen electro-sorption in the material may overlap with the above reported ones [29]. Actually, if the potential cut-off is lower than the thermodynamic limit for water reduction, nascent hydrogen is produced and weakly chemisorbed on the carbon surface [30]; correspondingly a hump due to hydrogen electro-oxidation appears during the anodic scan [29] and contributes to the overall capacitance. In Fig. 2 (right), LN600 displays anodic peaks at 0.75, −0.35 V and 0.75 V *vs* NHE in H_2SO_4, KOH and Na_2SO_4, respectively. Moreover, for the three electrolytes, in the region of anodic scan between the negative potential cut-off and the equilibrium potential for water reduction (Fig. 2, right), the anodic current is much lower for LN600 (being close to zero) than for LN750. It shows that, in this potential range, the EDL charging of LN600 is comparable to the redox current involved in water electro-reduction; by contrast for LN750, the EDL contribution is more important, that fits well with the larger specific surface area of this material.

Hydrogen chemisorption during water reduction is also at the origin of a noticeable over-potential for H_2 evolution, as demonstrated by the shift of the negative current leap (see Fig. 2, right). Whatever the electrolyte, the over-potential is higher for LN600, which contains a larger amount of oxygenated functionalities, than for LN750. Moreover, as it has been already observed for glassy carbon [31] or Pt [32] electrodes, the over-potential for H_2 evolution depends not only on the material used, but also on the electrolyte pH. In a neutral

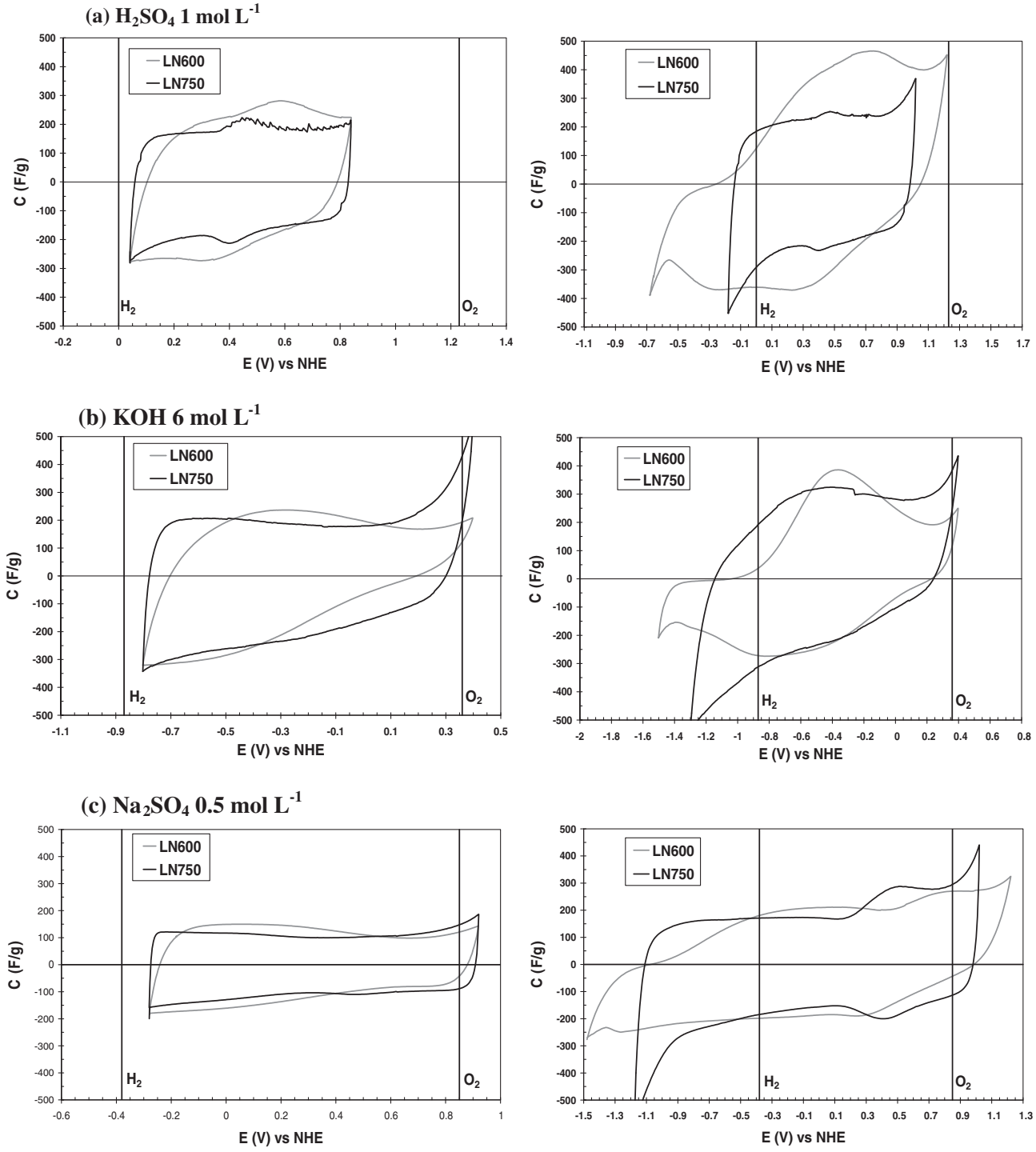

Fig. 2 – Cyclic voltammograms (2 mV s^{-1}) of LN600 and LN750 recorded in three-electrode cells with: (a) 1 mol L^{-1} H_2SO_4; (b) 6 mol L^{-1} KOH and (c) 0.5 mol L^{-1} Na_2SO_4.

pH solution, the over-potential observed with a glassy carbon electrode can reach 1.2 V, whereas only a value of 0.6 or 0.8 V is attained in acidic or basic pH, respectively. With a Pt electrode, a small over-potential of 0.3 V is found in neutral electrolyte, whereas any over-potential can be detected when using acidic or basic solutions. The LN600 nanoporous carbon, with a moderate surface area, but a high amount of oxygenated surface functionalities, presents almost the same over-potential values as glassy carbon in all the electrolytic media (see Fig. 2), confirming that the operating potential range in negative polarization is more important in a neutral Na_2SO_4 electrolyte whatever the electrode material.

Similarly, in Fig. 2 (right), the maximum positive potential depends both on the nature of the electrode material and on the electrolyte pH. The over-potential for O_2 evolution is more important for LN600 than for LN750 in H_2SO_4 and

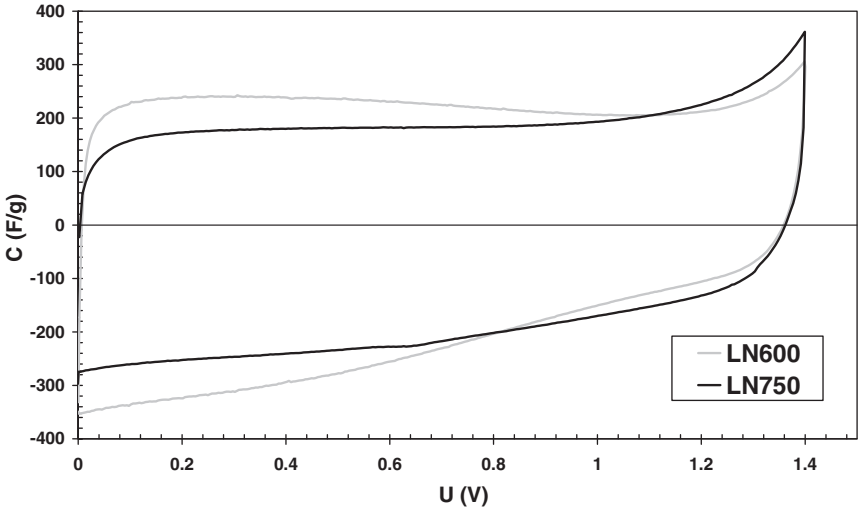

Fig. 3 – Cyclic voltammograms (2 mV s^{-1}) for LN600 and LN750 based symmetric capacitors in 6 mol L^{-1} KOH.

Na_2SO_4. When using glassy carbon [31] or Pt [32] electrodes, the anodic limit due to di-oxygen evolution can be more or less extended depending on the electrolyte pH. The highest oxygen over-potential has been observed in neutral solutions, with 0.7 or 0.5 V for glassy carbon or Pt electrodes, respectively, while it reaches smaller values in acidic and basic media, e.g., 0.5 and 0.3 V for glassy carbon and 0.0 and 0.4 V for Pt, respectively. However, Fig. 2a (right) shows that, in H_2SO_4, the oxidation of seaweed carbons takes place even before reaching the thermodynamic limit for di-oxygen evolution. This effect is shifted to a higher value for the more functionalized LN600. In KOH, the difference between the two materials is less marked (Fig. 2b, right). In Na_2SO_4, they can be polarized at potentials higher than the equilibrium potential for water oxidation, but the observed over-potentials are not as high as for glassy carbon or Pt electrodes, confirming that the nature of the electrode has an important role. In this sense, a higher content of oxygenated surface functionalities seems to favour a higher anodic limit. These results fit with Biniak et al. [26,33] observations, showing that a high oxygen content on the carbon surface ought to protect it from uncontrollable oxidation during electrochemical processes.

Taking into account the cathodic and anodic limits found in the different electrolytes for the seaweed carbons, it results clearly that the highest stability window can be attained in neutral solution. As it has been reported for the particular case of Pt [32], this property can be related to the fact that the H^+ and OH^- concentrations in neutral electrolyte are too low to induce gas evolution reactions.

In conclusion, the capacitance values and the stability potential window are both controlled by the nature of the electrode material and the electrolyte pH. The results exposed in Fig. 2 show that when using oxygen-rich seaweed carbons as electrodes, KOH or Na_2SO_4 can be good candidates for replacing the well performing but corrosive H_2SO_4 electrolyte. In particular, the large stability potential window of seaweed based carbons in neutral electrolyte – around 2.4 V for LN600 against 2 V for commercial activated carbons [24] – allows predicting supercapacitors operating up to a high voltage with a high energy density. However, the potential range of each individual electrode in a capacitor cell cannot be controlled. Therefore, in Section 3.2.3, it will be measured *vs* a reference electrode, and the cycleability of two-electrode cells will be investigated in order to determine the maximum operating voltage.

3.2.2. *Two-electrode cells performance in 6 mol L^{-1} KOH*

Fig. 3 shows the cyclic voltammograms of two-electrode cells with LN600 and LN750 based electrodes in 6 mol L^{-1} KOH. Despite the smaller specific surface area of LN600 compared to LN750, the former demonstrates a slightly higher capacitance. This fact together with the less rectangular shape of the CV for this capacitor confirm a higher pseudo-faradic contribution for LN600, what is logic on the basis of its richer surface functionality (Table 3).

The three-electrode cell CV presented in Fig. 2b suggest that voltage values around 1.7 V (stability potential window from −1.4 to 0.3 V *vs* NHE) and 1.4 V could be reached for capacitors based on LN600 and LN750, respectively.

Table 4 – Specific capacitance of LN600 and LN750 in two-electrode cells after 10 and 5000 galvanostatic (1 A g^{-1}) charge/discharge cycles up to different voltage values. Electrolyte: 6 mol L^{-1} KOH.

	LN600	LN600	LN600	LN750	LN750	LN750
Cell voltage (V)	0.8	1.0	1.2	1.2	1.4	1.6
C (F g^{-1}) after 10 cycles	166	175	159	168	163	140
C (F g^{-1}) after 5000 cycles	136	123	94	149	140	30
Capacitance loss (%)	18	30	41	11	14	79

Galvanostatic cycling of the two-electrode cells has been performed to assess the values of maximum voltage. Table 4 reports, for LN600 and LN750 based capacitors, the capacitance values obtained after 10 and 5000 charge/discharge cycles at 1 A g^{-1} up to different voltage values. After 10 cycles up to 0.8–1.2 V, the capacitance values of the two materials are very similar, e.g., 160–170 F g^{-1}. For comparison, using the same conditions in 1 mol L^{-1} H_2SO_4, the capacitance values are 180 and 220 F g^{-1} for LN750 and LN600, respectively. The smaller capacitance value for LN600 in KOH compared to H_2SO_4 is related to the already explained less efficient pseudo-faradic contribution of oxygenated surface functionalities in KOH medium [28].

For LN600, the capacitance loss after 5000 charge/discharge cycles up to 0.8 V is 18% (Table 4), demonstrating that 0.8 V is already a too high voltage, even if the cyclic voltammetry investigations (Fig. 3) suggested that 1.4 V could be reached. The capacitance decay may have two origins: (i) irreversible pseudo-faradic redox reactions and (ii) one of the two electrodes operating out of the stability potential window determined previously. In a two-electrode cell, the operating potential range of each electrode cannot be controlled and, beyond a given voltage, the potential of one of the electrodes can surpass the stability limits.

By contrast, the capacitor built with the LN750 carbon is able to operate up to 1.2 and 1.4 V with a capacitance loss of only 11% and 14%, respectively, after 5000 cycles. In other words, with this material, it is possible to take advantage of almost all the stability window determined in three-electrode configuration (see Fig. 2b). At 1.6 V, the capacitance decay is very high (Table 4) because this voltage is wider than the stability window of LN750 in KOH, and one electrode or both operate outside the stability window.

Whereas the oxygen rich LN600 seaweed based carbon demonstrated excellent performance in 1 mol L^{-1} H_2SO_4 [16], this is no longer the case in 6 mol L^{-1} KOH, due to the very low stability of the system during cycling. This phenomenon could be explained by an incomplete carbonization of the precursor leaving some amount of raw biopolymers non-carbonized, e.g., sodium alginate. This residual alginate is dissolved in the presence of the alkaline electrolyte [34] and the electrodes loose their integrity.

By contrast, with LN750 which contains a smaller amount of oxygenated surface functionalities, cell voltages of 1.2–1.4 V are attained in both H_2SO_4 and KOH media, with a good cycle life. Consequently, KOH can be a suitable electrolyte for high voltage seaweed carbon based supercapacitors in aqueous electrolyte, provided that the carbon electrode material is carefully selected.

3.2.3. *Two-electrode cells performance in 0.5 mol L^{-1} Na_2SO_4*

Fig. 4 shows the two-electrode cell voltammograms of LN600 and LN750 in 0.5 mol L^{-1} Na_2SO_4. Whereas the specific surface area of the two carbons is different, the capacitance values are quite similar for LN600 (125 F g^{-1}) and LN750 (123 F g^{-1}), because of their different surface functionalities. The values found are comparable to those obtained in three-electrode cell (Section 3.2.1).

Although Fig. 4 suggests that the LN600 and LN750 capacitors are able to operate up to 1.6 V, it is necessary to investigate the evolution of capacitance during galvanostatic cycling up to such voltage for claiming about a high stability of these systems. Fig. 5 shows the capacitance values *vs* the number of galvanostatic (1 A g^{-1}) charge/discharge cycles up to 1.6 V for the LN600 and LN750 based two-electrode cells in Na_2SO_4. In both cases, after a small capacitance drop during the first cycles, the values keep very stable during 10,000 cycles at 1.6 V. For comparison purposes, Fig. 5 includes the data obtained when cycling the LN600 and LN750 based supercapacitors at their maximum stability voltage in 6 mol L^{-1} KOH, e.g., 0.8 and 1.2 V, respectively, and in 1 mol L^{-1} H_2SO_4, e.g., 1.2 and 1.0 V, respectively. In spite of the lower capacitance values obtained in neutral electrolyte in comparison to the acidic or basic ones, the seaweed carbons based capacitors can be reversibly charged/discharged at much higher voltage in 0.5 mol L^{-1} Na_2SO_4. Table 5 summarizes the values of specific capacitance and maximum energy density for the LN600 and LN750 based supercapacitors, at the maximum voltage for

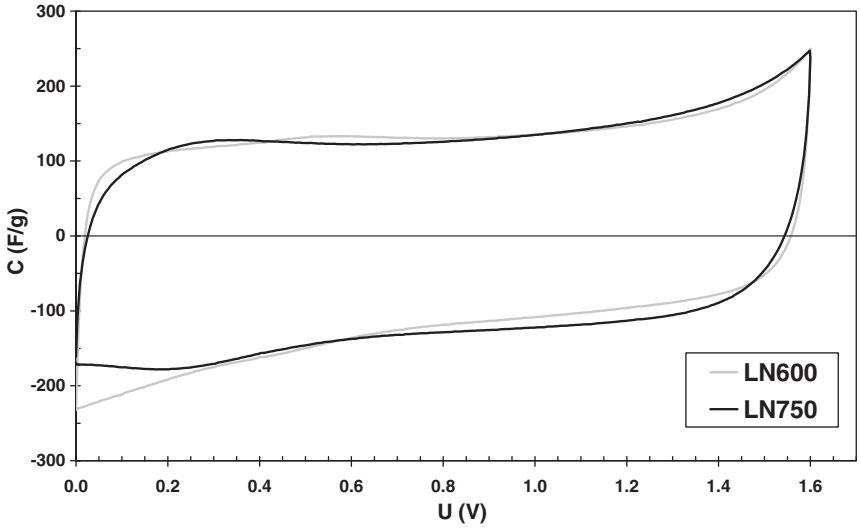

Fig. 4 – Cyclic voltammograms (2 mV s^{-1}) of LN600 and LN750 based symmetric capacitors in 0.5 mol L^{-1} Na_2SO_4.

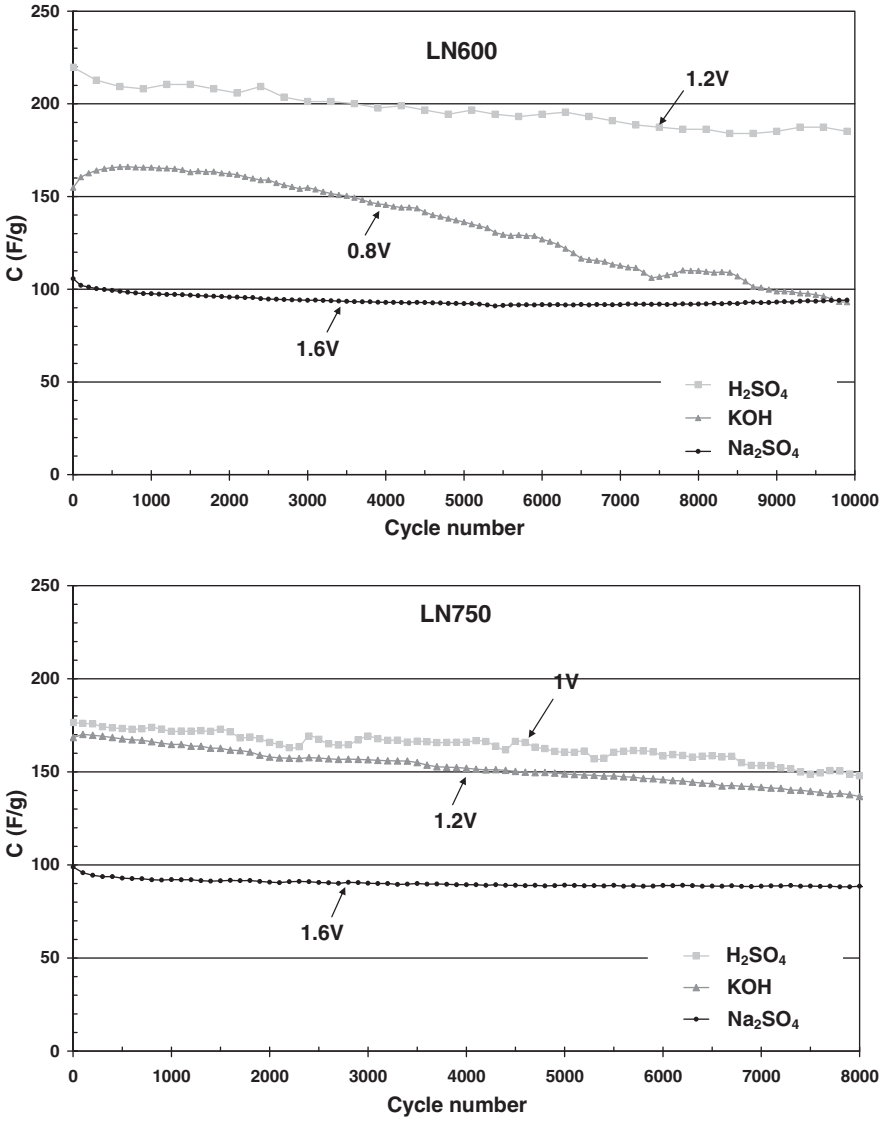

Fig. 5 – Evolution of capacitance during galvanostatic (1 A g^{-1}) cycling of LN600 and LN750 based supercapacitors in 0.5 mol L^{-1} Na_2SO_4, 6 mol L^{-1} KOH and 1 mol L^{-1} H_2SO_4.

which long term cycling has been demonstrated in the three electrolytes. It can be noticed that the energy density values of LN600 are comparable in H_2SO_4 and Na_2SO_4, and higher than in KOH. On the contrary, the energy density values of LN750 are comparable in KOH and Na_2SO_4 and higher than in H_2SO_4. Consequently, on the view point of storage performance, Na_2SO_4 appears as interesting electrolyte or even better than H_2SO_4 in presence of seaweed carbons, while being less corrosive.

Although 1.6 V is a very high voltage for a symmetric supercapacitor in aqueous electrolyte, Fig. 2c shows that the stability potential window of seaweed carbons can be as high

Table 5 – Electrochemical performance of LN600 and LN750 based supercapacitors using the three electrolytes.

Electrode material	Electrolyte	Cell voltage[a] (V)	C[b] (F g^{-1})	E_{max}[b] (Wh kg^{-1})
LN600	H_2SO_4	1.2	255	12.6
LN600	KOH	0.8	201	4.4
LN600	Na_2SO_4	1.6	125	10.7
LN750	H_2SO_4	1.0	179	6.2
LN750	KOH	1.2	188	9.4
LN750	Na_2SO_4	1.6	123	10.8

a Maximum voltage for long term cycling.
b Values obtained by galvanostatic discharge at 0.2 A g^{-1}.

as 2.4 V. In order to understand why such voltage value is not reached in a symmetric capacitor, the potential window of each electrode has been recorded while charging the cell up to different voltage values. For this experiment, a Hg/Hg_2SO_4 reference electrode has been introduced in the cell. Fig. 6 shows the evolution of the potential measured at $U = 0$ V (E_{0V}) and of the extreme electrode potentials E^+ and E^- *vs* various values of maximum voltage reached after the galvanostatic charge of supercapacitors based on LN600 and LN750. When the supercapacitor built with LN600 is charged up to $U = 1.6$ V, the positive electrode operates between 0.39 and 1.19 V *vs* NHE and the negative one between 0.39 and −0.41 V *vs* NHE. For the supercapacitor built with LN750 electrodes, in the same conditions, the positive electrode operates between 0.34 and 1.07 V *vs* NHE and the negative one between 0.34 and −0.53 V *vs* NHE. From these data, when the voltage of both capacitors reaches 1.6 V, the potential of the negative electrode is only slightly under the thermodynamic limit for water reduction, e.g., −0.38 V *vs* NHE. Consequently, one does not take full advantage of the pseudo-capacitive response related with hydrogen electrosorption, and more important, the entire stability window towards more negative potential values (see Fig. 2c) is underused. On the contrary, for the positive electrode, the potential values are as high as 1.19 and 1.07 V *vs* NHE for LN600 and LN750, respectively, while the theoretical value for water oxidation is 0.85 V *vs* NHE.

The anodic limit of the two materials was explored by recording their cyclic voltammograms in three-electrode cell up to very positive potential values (Fig. 7). The higher oxygen content on LN600 surface seems to enhance its oxidation resistance compared to LN750. While LN750 is extensively oxidized at potential values slightly higher than 1.1 V *vs* NHE (see the corresponding cathodic peak at around 0.45–0.50 V *vs* NHE), oxidation of LN600 is negligible at such potential values. Nevertheless, it is clear that the potential reached for the positive electrode in a LN600- or LN750-based supercapacitor charged up to 1.6 V is close to the one related to an irreversible oxidation of carbon. Therefore, it can be concluded that the maximum operating voltage of the capacitors is actually limited by the positive electrode.

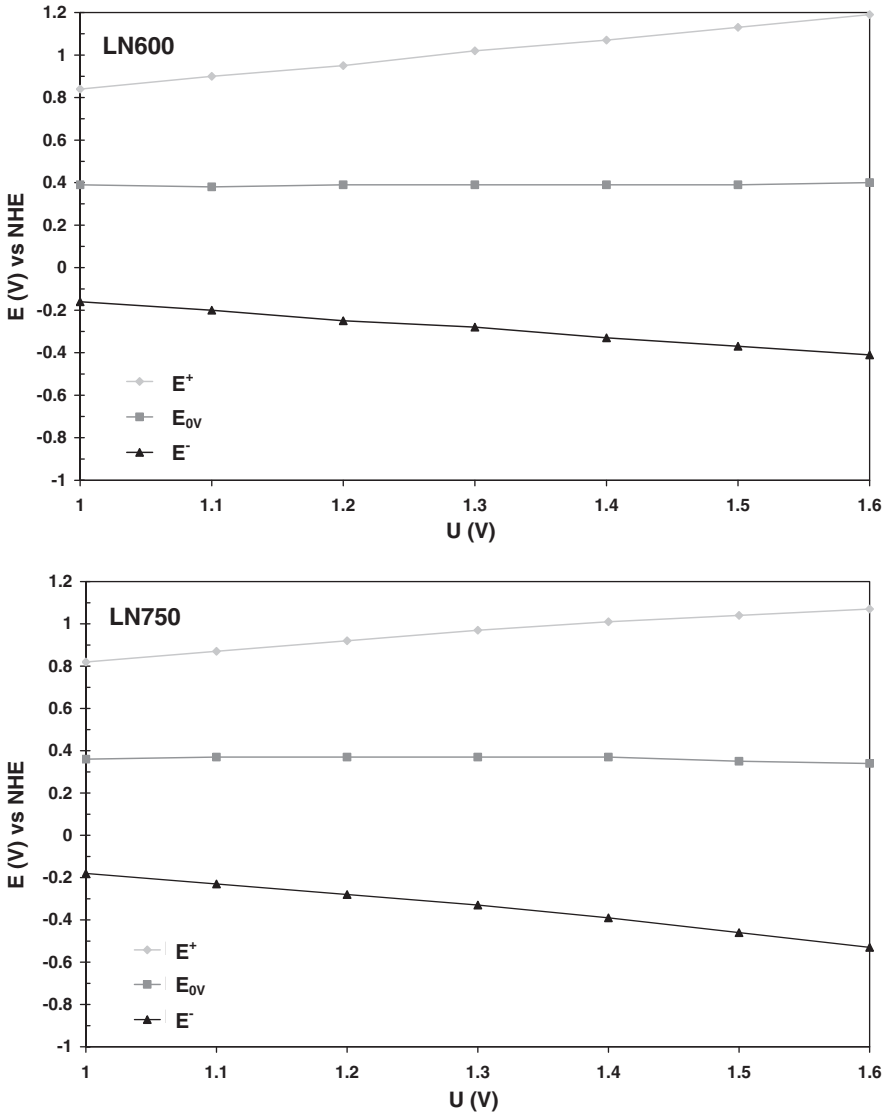

Fig. 6 – Evolution of the positive (E^+, light grey) and negative (E^-, dark) potential extrema while charging capacitors at 200 mA g^{-1} up to different voltage values. LN600 and LN750 electrodes in 0.5 mol L^{-1} Na_2SO_4.

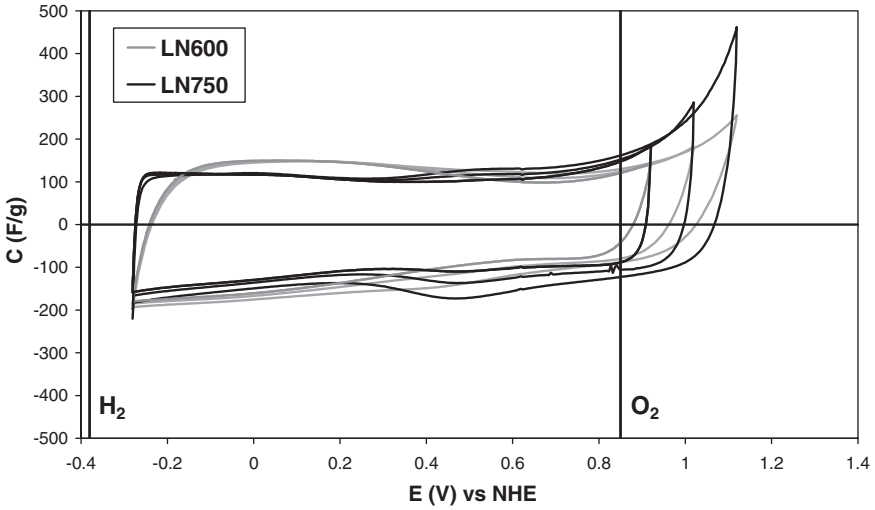

Fig. 7 – Three-electrode cell voltammograms (2 mV s^{-1}) of LN600 and LN750 with negative potential cut-off higher than the thermodynamic limit for water reduction. Electrolyte: 0.5 mol L^{-1} Na_2SO_4.

In summary, an exceptionally high voltage value of 1.6 V was reached with a symmetric carbon/carbon capacitor in Na_2SO_4 aqueous electrolyte by using seaweed carbons. However, the offered possibilities of extending the negative electrode potential towards more negative values could not be fully exploited in this configuration.

4. Conclusion

Seaweed carbons have been electrochemically characterized as electrode for supercapacitors in KOH, H_2SO_4 and Na_2SO_4 aqueous electrolytes. The nature of the electrode material and the electrolyte pH influence both the capacitance values and the stability potential window. For a particular electrolyte, the carbon with the highest oxygen content demonstrates the highest capacitance values and stability potential window. A very high value of 2.4 V was observed for the stability potential window of this carbon in Na_2SO_4 solution. Moreover, it has been shown for the first time that a contribution of pseudo-faradic reactions is possible in a neutral electrolyte if the material posses an adequate surface functionality. In particular, the quinone-like groups seem to be the most active ones.

It was demonstrated that a symmetric carbon/carbon cell can operate up to 1.6 V in Na_2SO_4 aqueous electrolyte. This performance shows that a neutral aqueous electrolyte is very attractive for developing a new generation of environment friendly carbon/carbon supercapacitors able to compete with the organic electrolyte based systems.

REFERENCES

[1] Frackowiak E, Béguin F. Carbon materials for the electrochemical storage of energy in capacitors. Carbon 2001;39:937–50.
[2] Miller JR, Simon P. Electrochemical capacitor design for energy management. Science 2008;321:651–2.
[3] Kotz R, Carlen M. Principles and applications of electrochemical capacitors. Electrochim Acta 2000;45:2483–98.
[4] Conway BE. Electrochemical supercapacitors : scientific fundamentals and technological applications. New York: Kluwer Academic Publishers/Plenum Press; 1999.
[5] Ruiz V, Santamaría R, Granda M, Blanco C. Long term cycling of carbon based supercapacitors in aqueous media. Electrochim Acta 2009;54:4481–6.
[6] Conway BE, Birss V, Wojtowicz J. The role and utilization of pseudocapacitance for energy storage by supercapacitors. J Power Sources 1997;66:1–14.
[7] Hsieh CT, Teng H. Influence of oxygen treatment on electric double-layer capacitance of activated carbon fabrics. Carbon 2002;40:667–74.
[8] Okajima K, Ohta K, Sudoh M. Capacitance behavior of activated carbon fibers with oxygen-plasma treatment. Electrochimica Acta 2005;50:2227–31.
[9] Nian YR, Teng H. Influence of surface oxides on the impedance behaviour of carbon-based electrochemical capacitors. J Electroanal Chem 2003;540:119–27.
[10] Jurewicz K, Pietrzak R, Nowicki P, Wachowska H. Capacitance behaviour of brown coal based active carbon modified through chemical reaction with urea. Electrochimica Acta 2008;53:5469–75.
[11] Dong YR, Nishiyama N, Kodama M, Egashira Y, Ueyama K. Nitrogen-containing microporous carbons prepared from anionic surfactant-melamine/formaldehyde composites. Carbon 2009;47:2138–42.
[12] Hulicova D, Kodama M, Hatori H. Electrochemical performance of nitrogen enriched carbons in aqueous and non-aqueous supercapacitors. Chem Mater 2006;18:2318–26.
[13] Raymundo-Piñero E, Leroux F, Béguin F. A high performance carbon for supercapacitors obtained by carbonization of a seaweed biopolymer. Adv Mater 2006;18:1877–82.
[14] Kodama M, Yamashita J, Soneda Y, Hatori H, Nishimura S, Kamegawa K. Structural characterization and electric double layer capacitance of template carbons. Mater Sci Eng B 2004;108:156–61.
[15] Rufford TE, Hulicova-Jurcakova D, Zhu Z, Lu GQ. Nanoporous carbon electrode from waste coffee beans for high performance supercapacitors. Electrochem Commun 2008;10:1594–7.

[16] Raymundo-Piñero E, Cadek M, Béguin F. Tuning carbon materials for supercapacitors by direct pyrolysis of seaweeds. Adv Funct Mater 2009;19:1032–9.
[17] Linden D, Reddy TB. Handbook of batteries. 3rd ed. New York: Mc Graw-Hill; 2002.
[18] Brousse T, Taberna PL, Crosnier O, Dugas R, Guillemet P, Scudeller Y, et al. Long-term cycling behavior of asymmetric activated carbon/MnO_2 aqueous electrochemical supercapacitor. J Power Sources 2007;173:633–41.
[19] Khomenko V, Raymundo-Piñero E, Béguin F. Optimisation of an asymmetric manganese oxide/activated carbon capacitor working at 2 V in aqueous medium. J. Power Sources 2006;153:183–90.
[20] Hu CC, Wang CC, Wu FC, Tseng RL. Characterization of pistachio shell-derived carbons activated by a combination of KOH and CO_2 for electric double layer capacitors. Electrochimica Acta 2007;52:2498–505.
[21] Subramanian V, Luo C, Stephan AM, Nahm KS, Thomas S, Wei B. Supercapacitors from activated carbon derived from banana fibers. J Phys Chem C 2007;111:7527–31.
[22] Qu QT, Wang B, Yang LC, Shi Y, Tian S, Wu YP. Study on electrochemical performance of activated carbon in aqueous Li_2SO_4, Na_2SO_4 and K_2SO_4 electrolytes. Electrochem Commun 2008;10:1652–5.
[23] Konno H, Ito T, Ushiro M, Fushimi K, Azumi K. High capacitance B/C/N composites for capacitor electrodes synthesized by a simple method. J Power Sources 2010;195:1739–46.
[24] L. Demarconnay, E. Raymundo-Piñero, F. Béguin. A symmetric carbon/carbon supercapacitor operating at 1.6 V by using a neutral aqueous solution. Electrochem Commun 2010, doi: 10.1016/j.elecom.2010.06.036.
[25] Cazorla-Amorós D, Alcañiz-Monge J, de la Casa-Lillo MA, Linares-Solano A. CO_2 as an adsorptive to characterize carbon molecular sieves and activated carbons. Langmuir 1998;14:4589–96.
[26] Boehm HP, Voll M. Basische oberflachenoxide auf kohlenstoff I Adsorption von sauren. Carbon 1970;8:227–40.
[27] Biniak S, Swiatkowski A, Pakula M. Electrochemical studies of phenomena at active carbon-electrolyte solution interfaces. In: Radovic LR, editor. Chemistry and physics of carbon, vol 27. New York: Dekker Inc.; 2001. p. 125–225.
[28] Andreas HA, Conway BE. Examination of the double-layer capacitance of an high specific-area C-cloth electrode as titrated from acidic to alkaline pHs. Electrochimica Acta 2006;51:6510–20.
[29] Jurewicz K, Frackowiak E, Béguin F. Towards the mechanism of electrochemical hydrogen storage in nanostructured carbon materials. Appl Phys A 2004;78:981–7.
[30] Béguin F, Friebe M, Jurewicz K, Vix-Guterl C, Dentzer J, Frackowiak E. State of hydrogen electrochemically stored using nanoporous carbons as negative electrode materials in an aqueous medium. Carbon 2006;44:2392–8.
[31] Wang J, Kirgoz UA, Mo JW, Lu J, Kawde AN, Muck A. Glassy carbon paste electrodes. Electrochem Commun 2001;3:203–8.
[32] Hong MS, Lee SH, Kim SW. Use ok KCl aqueous electrolyte for 2V manganese oxide/activated carbon hybrid capacitor. Electrochem Solid State Lett 2002;5:A227–30.
[33] Swiatkowski A, Pakula M, Biniak S. Cyclic voltammetric studies of chemically and electrochemically generated oxygen species on activated carbons. Electrochimica Acta 1997;42:1441–7.
[34] McHugh DJ. A guide to the seaweed industry. FAO fisheries technical paper 441; 2003. p. 39–49.